Laboratory Based X-ray Absorption Spectroscopy of Iron Phosphate Glasses for Radioactive Waste Immobilisation: A Preliminary Investigation

L M Mottram,[1] M C Stennett,[1] S K Sun[1] and N C Hyatt[1]*

Department of Materials Science & Engineering, The University of Sheffield, Mappin Street, Sheffield, S1 3JD.

*n.c.hyatt@sheffield.ac.uk

Abstract. We report the application of laboratory based X-ray absorption spectroscopy to the speciation of Fe in iron phosphate glasses prepared by conventional and microwave melting. Analysis of the weak pre-edge features in Fe K-edge XANES data demonstrated glasses produced by microwave melting to have a higher fraction of reduced Fe^{2+} species, since microwave melts do not have sufficient time to equilibrate with the prevailing oxygen partial pressure, compared to counterparts produced by conventional melting. Furthermore, our laboratory XANES data are consistent with the formation of octahedral Fe^{2+} at the expense of tetrahedral Fe^{3+} species, with increasing Fe^{2+} content. These findings are consistent with the previous findings of our [57]Fe Mossbauer study, synchrotron XANES data, and current understanding of the structure of iron phosphate glasses, and demonstrate the utility of laboratory based XANES for routine speciation of Fe in these and other materials.

1. Introduction

The baseline treatment option for intermediate level wastes in the UK is encapsulation in an ordinary portland cement matrix, combined with super-compaction, where appropriate. However, there is a growing appreciation that some wastes, such as reactive metals and organic materials, are not compatible with this approach [1-3]. Furthermore, cement encapsulation technology results in a dilution of the radioactive waste feed and a projected increase in the packaged waste volume by typically 30%. In principal, thermal treatment technologies challenge these shortcomings, through at least partial oxidation of metallic and organic waste components, to produce a passively safe product, with retention of radioactive and chemotoxic elements [3-10].

Iron phosphate glasses are one matrix of interest for the vitrification of some challenging radioactive wastes [11-13]. The $40Fe_2O_3$–$60P_2O_5$ (mol%) glass composition, has been extensively studied for radioactive waste immobilisation, due to the high incorporation rate of elements which have low solubility in borosilicate melts (e.g. F, Cl, S and Bi), good chemical durability, and reasonable processing temperature and melt viscosity [14-16].

X-ray absorption and [57]Fe Mossbauer spectroscopy studies of iron phosphate glasses have demonstrated the Fe^{2+} / Σ Fe ratio to be sensitive to melt composition and processing conditions (temperature, time and atmosphere) [16-19]. This redox ratio is determined by the equilibrium: $2\,FeO_{(melt)} + \tfrac{1}{2}\,O_{2\,(g)} = Fe_2O_{3\,(melt)}$, and, in the case of the $40Fe_2O_3$–$60P_2O_5$ glass composition, up to 60% of the total Fe may be present as Fe^{2+} [17]. An increased fraction of Fe^{2+} is reported to be both detrimental to glass forming ability and radiation stability [16, 19-22], whereas chemical durability is

reported to be insensitive to the fraction of Fe^{2+} [18]. The Fe^{2+} / Σ Fe ratio also governs the electrical conductivity of Fe_2O_3-P_2O_5 glass melts, which is an important consideration for some melter designs, in the context of application to radioactive waste treatment [19].

From the preceding discussion, it will be appreciated that routine determination of Fe^{2+} / Σ Fe ratio in Fe_2O_3-P_2O_5 glasses is of importance for formulation and development of such waste forms. ^{57}Fe Mossbauer spectroscopy has been widely exploited for the determination of Fe^{2+} / Σ Fe ratio, according to the distinctive isomer shift and quadrupole splitting of Fe^{2+} and Fe^{3+} species, which are also sensitive to co-ordination number [13, 16-18, 23]. However, the determination of average Fe co-ordination number is complicated by the overlap of ^{57}Fe isomer shift and quadrupole splitting ranges, particularly for amorphous materials [13, 23]. Whilst ^{57}Fe Mossbauer spectroscopy can conveniently be applied in a laboratory environment, data acquisition is dependent on ^{57}Fe concentration, ^{57}Co source activity, and sample characteristics, which translate to data acquisition time of days per sample.

Fe K-edge X-ray absorption spectroscopy has also been applied to determination of Fe^{2+} / Σ Fe ratio in Fe_2O_3-P_2O_5 glasses. The weak pre-edge features in the Fe K-edge X-ray Absorption Near Edge Structure (XANES), located ca. 15–20 eV below the edge step, have been shown to be a sensitive probe of Fe speciation [24-29]. These features are associated with 1s – 3d (quadrupole) and/or 1s – 4p (dipole) electronic transitions in the Fe absorber atom and, therefore, are sensitive to both the electronic configuration and symmetry, from which oxidation state and co-ordination number are inferred. Wilke *et al.* developed a systematic methodology to extract the normalised pre-edge features from Fe K-edge XANES data and determination of the centroid energy position and total integrated intensity, which were effectively correlated with Fe oxidation state and co-ordination number [27, 28]. Conventionally, acquisition of XANES data has required access to a synchrotron radiation beamline, which is highly competitive, time limited, and not immediate. Recently, however, we demonstrated the first proof of concept Fe K-edge XANES speciation studies, using a commercially available laboratory X-ray spectrometer, from analysis of weak pre-edge features [30]. This approach enables routine Fe speciation in materials with data acquisition times of only a few hours. Here, we build on this recent study to demonstrate the potential for Fe redox determination in $40Fe_2O_3$–$60P_2O_5$ glasses prepared by conventional and microwave melting. Our preliminary results demonstrate that laboratory based Fe K-edge XANES has sufficient resolution and sensitivity to routinely determine Fe^{2+} / Σ Fe ratio in iron phosphate glasses.

2. Experimental

2.1. Synthesis of iron phosphate glasses
Iron phosphate glasses of $40Fe_2O_3$–$60P_2O_5$ (mol%) composition were prepared by conventional and microwave heating, as previously described [23, 31, 32]. Conventional melting used a stoichiometric mixture of Fe_3O_4 and P_2O_5 (PO) or $NH_4H_2PO_4$ (AP), in covered silica crucibles, heated at 1150°C for 5h in air. Microwave melting used a stoichiometric mixture of Fe_3O_4 and P_2O_5 or $NH_4H_2PO_4$, in covered silica crucibles, heated for 12 minutes at 800W power in a domestic microwave oven (DMO). Fe_3O_4 was selected as the iron source since it is known to strongly couple to the 2.45 GHz frequency of domestic microwaves, resulting in rapid self heating. After approximately 20 seconds of microwave irradiation a dull red glow emanating from the crucible was observed through the silica lid. The intensity of the glow increased until, after approximately 1 minute, an incandescent red glow could be clearly observed. This continued until the DMO was switched off. The peak temperature of melting was estimated to be 1150°C, using a grounded thermocouple. Glasses were quenched in air and confirmed to be amorphous by X-ray diffraction.

2.2. Reference compounds
Fe K-edge XANES data were acquired from four selected reference compounds. $NaFeSi_2O_6$ (aegirine) and Fe_2SiO_4 (fayalite) are characterised by Fe^{3+} and Fe^{2+}, respectively, in octahedral FeO_6 co-ordination (CN = 6); whereas $FePO_4$ and $Fe_{1.5}Mg_{0.5}Al_{9.1}Si_{3.9}(OH)_2$ (staurolite) are characterised by Fe^{3+} and Fe^{2+}, respectively, in tetrahedral FeO_4 co-ordination (CN = 4) [33-36]. Polycrystalline $FePO_4$ and Fe_2SiO_4

were, respectively, synthesised by: solid state reaction of Fe_2O_3 and $NH_4H_2PO_4$ at 900 °C in air for 16 h; and solid state reaction of stoichiometric quantities of Fe, Fe_2O_3 and SiO_2 at 750 °C for 48 h in a sealed, evacuated, quartz tube. Mineral specimens of aegirine (Langesund Fjord, Norway), and staurolite (Georgia, USA), were provided from our own collection. All materials were confirmed to be single phase by powder X-ray diffraction. The expected Fe speciation was verified by [57]Fe Mossbauer analysis.

2.3. Fe K-edge XANES

Fe K-edge XANES data were acquired on an EasyXAFS XES100 spectrometer, Figure 1, based on the design of Seidler *et al.*, equipped with an air cooled X-ray tube operating at 25 kV and 4 mA, with a Hitatchi Vortex Silicon Drift Detector (SDD) [37-40]. The spectrometer was configured with a Ge (620) SBCA to scan the energy range 6970 – 7340 eV, with a step size of 0.25 eV and constant count time of 4s / point in the XANES region (total scan time 30 min per data set). The energy resolution of the SDD is ca. 140 eV, enabling rejection of the harmonic content of the incident beam and background scatter. A He flight-path was used to minimise air scatter and absorption. Transmission data were acquired with ($I_t(E)$) and without the sample ($I_0(E)$), using the same scan parameters. The Ge (620) monochromator was aligned using the clock angle procedure of Mortensen and Seidler, to account for the crystal miscut [41]. Data integration time was typically 4h per spectrum.
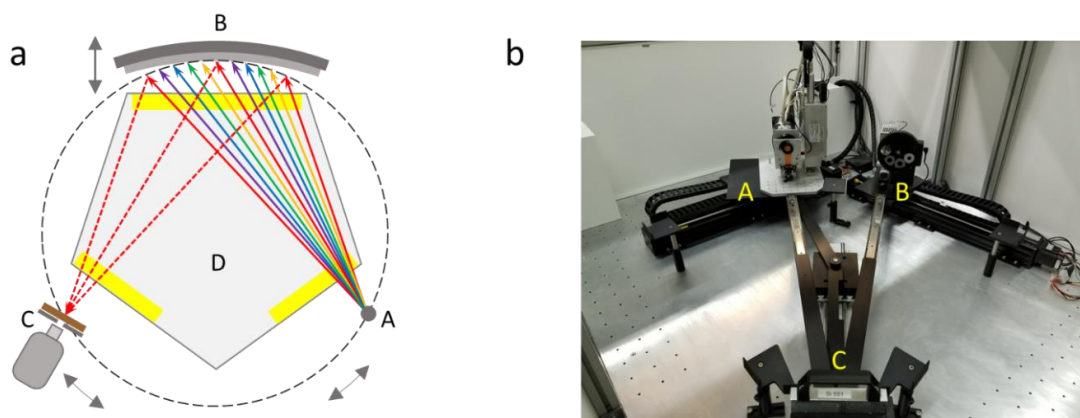

Figure 1. a) Schematic representation of Rowland circle geometry for laboratory transmission X-ray Absorption Spectroscopy, as described in the text, showing: broadband low power X-ray source (A); spherically bent crystal analyser (B); sample / detector assembly (C); and helium filled beam path with kapton windows (D); **b)** Photograph of EasyXAFS XES100 spectrometer arrangement shown in Fig. 1a, with helium filled beam path removed, to show linear translation stages and steering bars used to maintain alignment of X-ray source (A), analyser (B), and sample / detector assembly (C).

Fe K-edge XANES data were also acquired on the KMC-2 beamline at the BESSY-II synchrotron. The KMC-2 beamline is situated on a bending magnet and was configured with a Si (111) channel cut monochromator and mirror for harmonic rejection. Incident and transmitted beam intensities were measured using ionization chambers, filled with mixtures of He and N_2, operated in a stable region of their I/V curve. For synchrotron data, a step size of 0.25 eV was used in the XANES region with a count time of 1s / point. Data integration time was typically 0.5h per spectrum.

Samples were prepared from finely ground specimens of glasses or reference compounds dispersed in 70 mg of polyethylene glycol, pressed into 13 mm diameter pellets, to achieve a thickness of one absorption length. Data reduction and analysis was performed using the programs Athena and Hephaestus [42]. Calibration of the energy scale were achieved by reference to a 5 μm Fe foil (Goodfellow Cambridge Ltd.), for which the first peak in the derivative spectrum was set to 7112.00 eV, as defined by Bearden and Burr for the Fe K absorption edge [43]. Data from the reference foil

were acquired periodically for the laboratory and synchrotron experiments, the absolute energy scale for the laboratory XANES data was calibrated as previously described [30, 44].

Extraction and analysis of the pre-edge feature in Fe K-edge XANES data were achieved using Microsoft Excel software, to first fit a spline function to model and subtract the contribution of the edge step. The pre-edge envelope was then deconvoluted by fitting Gaussian components using a linear least squares refinement to optimise the normalised height, full width at half height, and energy position, so as to minimise the difference between the observed and calculated envelope determined from the sum of the fitted Gaussian components. Fitting initially utilised two Gaussian components with the significance of a third component tested by inspection of the improvement in goodness of fit. The total integrated intensity and centroid energy of the pre-edge feature were determined, respectively, from the sum of the integrated intensities and intensity weighted average energy position of the Gaussian components. The same initial parameters were used for all data sets, and several sets of different initial parameters trialled, to ensure that convergence did not arise in a local minimum. This approach is a simplification of that applied by Wilke *et al.*, which employed pseudo-Voigt components [28, 30].

3. Results and discussion

Figure 2 shows a head to head comparison of Fe K-edge XANES data acquired from $40Fe_2O_3$–$60P_2O_5$ (mol%) glasses, where, respectively, C and M are used to denote materials processed by conventional and microwave heating, and PO and AP denote the use of P_2O_5 and $NH_4H_2PO_4$ reagents. Excellent correspondence is observed between the laboratory (points) and synchrotron (solid line) XANES data, demonstrating that acquisition of good quality Fe K-edge XANES data using the laboratory set up, with reasonable data integration times. Note that the synchrotron data have *not* been convoluted by Gaussian or Lorentzian broadening for this comparison.
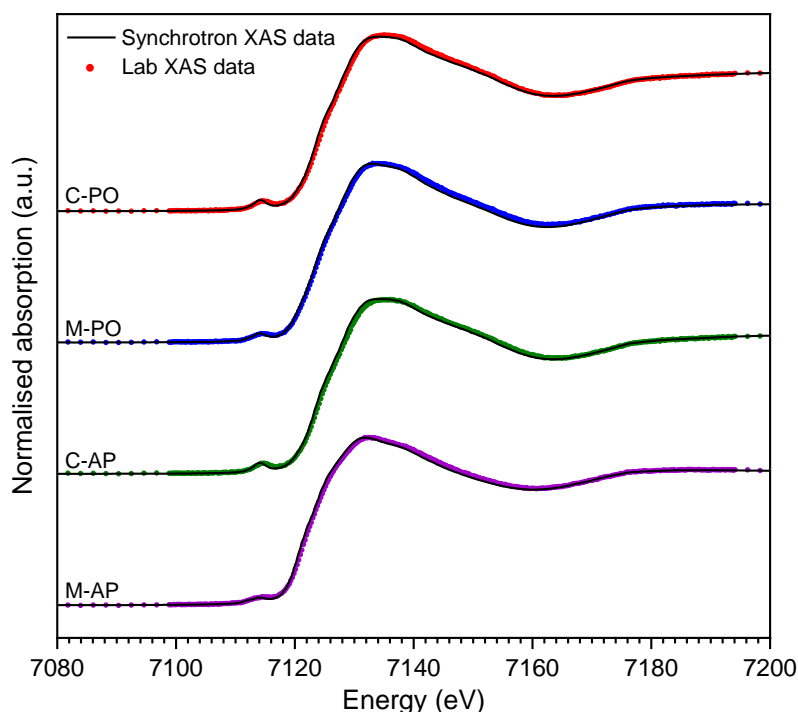

Figure 2. Comparison of normalised transmission mode Fe K-edge XANES spectra from $40Fe_2O_3$–$60P_2O_5$ glasses prepared by microwave (M) or conventional (C) heating of Fe_3O_4 with P_2O_5 (PO) or $NH_4H_2PO_4$ (AP), acquired using laboratory XAS spectrometer (points) and KMC-2 synchrotron beamline (solid line).

Figure 3 shows the extracted pre-edge features from the laboratory XANES data of the glass samples and the modelled envelope of the Gaussian components. Although the laboratory data show some scatter, as a result of the relatively low signal to noise ratio, the pre-edge features are evidently resolvable and measurable relative to the background. For each material, the pre-edge features of the laboratory and synchrotron XANES data were adequately modelled using three Gaussian components, the fitted parameters are summarised in Table 1. The fitted centroid position and integrated intensity of the pre-edge features are plotted in Figure 4, together with data from the reference compounds analysed in this study and that of Wilke *et al.* [28]. Note that the data of Wilke *et al.* (calibrated to $E_0 = 7111.08$ eV), were shifted by +0.92 eV, consistent with our absolute energy scale.
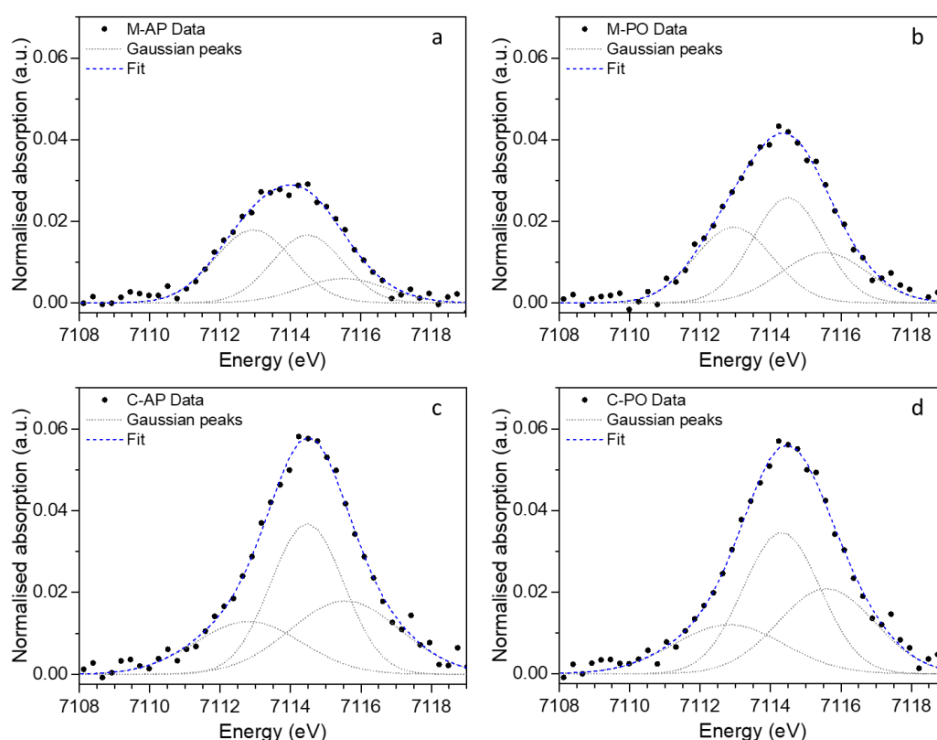

Figure 3. Normalised pre-edge spectra at Fe K edge (points) from $40Fe_2O_3$–$60P_2O_5$ glasses prepared by microwave (M) or conventional (C) heating of Fe_3O_4 with P_2O_5 (PO) or $NH_4H_2PO_4$ (AP), acquired using laboratory XAS spectrometer (points), showing fitted Gaussian components (grey dotted line) and their summation envelope (blue dotted line).

Table 1. Integrated intensity and centroid energy for Gaussian components fitted to pre-edge features of $40Fe_2O_3$–$60P_2O_5$ glasses prepared by microwave (M) or conventional (C) heating of Fe_3O_4 with P_2O_5 (PO) or $NH_4H_2PO_4$ (AP). Values in bold type are derived from laboratory data; values in normal type are derived from synchrotron data.

Sample	Gaussian 1		Gaussian 2		Gaussian 3		Centroid	Total
	Energy (eV)	**Intensity (a.u.)**	**Energy (eV)**	**Intensity (a.u.)**	**Energy (eV)**	**Intensity (a.u.)**	**Energy (eV)**	**integrated intensity (a.u)**
C-AP	**7112.8**	**0.049**	**7114.5**	**0.096**	**7115.5**	**0.070**	**7114.4**	**0.215**
	7112.9	0.046	7114.4	0.103	7115.4	0.068	7114.4	0.217
C-PO	**7112.8**	**0.047**	**7114.3**	**0.095**	**7115.6**	**0.072**	**7114.4**	**0.213**
	7112.8	0.049	7114.3	0.120	7115.5	0.043	7114.3	0.212
M-AP	**7113.0**	**0.049**	**7114.5**	**0.042**	**7115.5**	**0.018**	**7114.0**	**0.110**
	7112.4	0.041	7114.4	0.073	7115.5	0.002	7113.7	0.116
M-PO	**7113.0**	**0.051**	**7114.5**	**0.065**	**7115.5**	**0.038**	**7114.2**	**0.154**
	7112.8	0.045	7114.3	0.094	7115.5	0.021	7114.1	0.160

As shown in the speciation plot of Figure 4, the data points for the Fe^{3+} reference compounds $NaFeSi_2O_6$ (octahedral, FeO_6) and $FePO_4$ (tetrahedral, FeO_4) are in excellent agreement between the laboratory data (solid blue circles) and synchrotron data (solid red circles), and the data reported by Wilke *et al.* (solid black circles) [28]. The Fe^{2+} reference compounds $Fe_{1.5}Mg_{0.5}Al_{9.1}Si_{3.9}(OH)_2$ (octahedral, FeO_6) and Fe_2SiO_4 (tetrahedral, FeO_4) were investigated using only the laboratory set up, but these data (solid blue circles) but are also in reasonable agreement with the data reported by Wilke *et al.* (solid black circles) [28]. Both the laboratory and synchrotron data points fall within the known field for Fe^{2+} / Fe^{3+} speciation for octahedral (CN = 6) and tetrahedral (CN = 4) co-ordination, defined by the reference compounds reported by Wilke *et al.* (solid / open black circles). Figure 4 demonstrates that laboratory XANES is effective in distinguishing Fe^{2+} and Fe^{3+} species according to the centroid of the pre-edge features at 7112.9 ± 0.1 eV and 7114.5 ± 0.1 eV respectively. The chemical shift between the centroid energy of Fe^{2+} and Fe^{3+} species determined in this investigation was thus 1.6 ± 0.1 eV for laboratory XANES data, which is in excellent agreement with the value of 1.4 ± 0.1 eV determined by Wilke *et al.* and our previous feasibility study [28, 30]. Figure 4 demonstrates that laboratory XANES is also effective in differentiating tetrahedral and octahedral Fe^{2+} / Fe^{3+} species, according to the relative total integrated intensity of the pre-edge feature. As noted above, the pre-edge feature is associated with $1s - 3d$ quadrupole transitions, which are only weakly allowed for a centrosymmetric octahedral environment but have enhanced transition probability in non-centrosymmetric tetrahedral environments, due to admixture of unoccupied 4p orbitals in the final state.
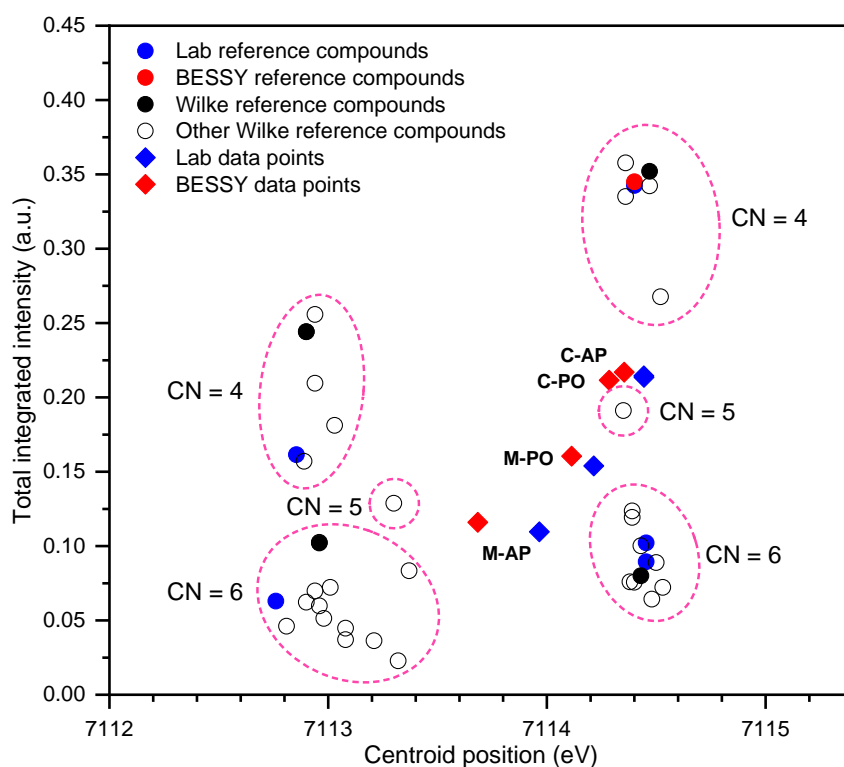

Figure 4. Speciation field diagram, based on total integrated intensity and centroid energy of pre-edge feature of Fe K-edge XANES data. Data points derived from analysis of our laboratory XANES are shown by solid blue circles (reference compounds) or diamonds (glasses); data points derived from synchrotron XANES are shown as solid red circles (reference compounds) or diamonds (glasses); equivalent data points of reference compounds from Wilke *et al.*, are shown as solid black circles (other reference data from Wilke *et al.*, shown as open black circles) [28]. Note data from Wilke *et al.*, are shifted by +0.92 eV consistent with our absolute energy scale as described in the text.

Turning to the analysis of the $40Fe_2O_3$–$60P_2O_5$ glass compositions, Figure 4 shows reasonably good agreement between the laboratory and synchrotron data points, demonstrating that laboratory XANES has, in principle, sufficient resolution and sensitivity to probe Fe^{2+} / Σ Fe ratio in iron phosphate glasses. The centroid energy of the pre-edge feature of glasses produced by microwave heating (M) is displaced toward lower energy compared to glasses produced by conventional melting (C), implying the presence of a greater concentration of Fe^{2+} species in the microwave processed materials. This is in agreement with our previous [57]Fe Mossbauer investigation [23], which estimated the Fe^{2+} / Σ Fe ratio to be 0.43 for glass M-AP, 0.22 for glass M-PO, and 0.10 for glass C-AP and C-PO. The centroid position of the pre-edge feature is known to show a non-linear dependence on Fe^{2+} / Σ Fe ratio, when both average oxidation state and co-ordination number vary at the same time [28], which is clearly inferred in this case from Figure 4 (see below). Hence, the Fe^{2+} / Σ Fe ratio cannot yet be reliably estimated from our XANES data without further careful calibration using mixtures of reference compounds. Nevertheless, it is evident from Figure 4 that glasses produced by microwave heating are characterised by a higher Fe^{2+} / Σ Fe redox ratio compared to the counterparts prepared by conventional melting. The higher Fe^{2+} / Σ Fe ratio for the microwave processed glasses, previously demonstrated by [57]Fe Mossbauer spectroscopy [23], is a reflection of the rapid processing time, which does not allow the melt to reach equilibrium with the prevailing oxygen partial pressure, compared to the conventionally processed counterparts. It is also evident from Figure 4, that the highest Fe^{2+} / Σ Fe ratio is observed for the microwave processed glass using $NH_4H_2PO_4$ as the phosphate source, also in agreement with our earlier [57]Fe Mossbauer investigation [23]. Decomposition of $NH_4H_2PO_4$ during the rapid microwave heating evolves NH_3 gas which maintains a sufficiently reducing environment to assist incorporation of Fe^{2+} within the melt, potentially also inducing partial reduction of Fe^{3+}. It is notable that the synchrotron determined data points in Figure 4 (red diamonds) are displaced to slightly higher centroid energy, compared to those determined by laboratory analysis (blue diamonds) on the same glass materials. This may suggest a small systematic difference in Fe^{2+} / Σ Fe ratio determined by laboratory and synchrotron XANES, however, this should be considered with due caution given the expected non-linear dependence of centroid energy on Fe^{2+} / Σ Fe ratio, which must be determined for both data sets.

Figure 4 also reveals a measurable difference of average Fe co-ordination in the microwave and conventionally melted glasses. In the case of conventionally melted glasses, the integrated intensity of the pre-edge feature implies a mixture of tetrahedral and octahedral, and/or pentahedral, Fe^{3+} species are present. This is in agreement with more recent Fe K-edge synchrotron XANES and [57]Fe Mossbauer studies of iron phosphate glasses, which point to a mixture of tetrahedral and octahedral, and or pentahedral, Fe^{3+} species, when Fe^{2+} / Σ Fe < 0.2 [13, 45, 46]. The microwave processed glasses are characterised by pre-edge features of lower integrated intensity, compared to their conventionally processed counterparts. This implies that the higher Fe^{2+} / Σ Fe ratio of the microwave processed glasses is associated with an increased proportion of octahedral Fe^{2+} (which would be expected to prefer octahedral co-ordination on the basis of crystal field stabilisation energy). This observation is consistent with the current understanding of the structure of iron phosphate glasses, in which an increase in Fe^{2+} / Σ Fe ratio, results in conversion of network forming tetrahedral Fe^{3+} to network modifying octahedral Fe^{2+} polyhedra [13,45,46]. Further work to accurately estimate the Fe^{2+} / Σ Fe ratio using mixtures of reference compounds, should also allow the proportion of co-ordination environments to be determined from laboratory XANES data,

4. Conclusions

Analysis of the weak pre-edge features in Fe K-edge XANES data from a laboratory XAS spectrometer demonstrated microwave processed iron phosphate glasses to incorporate a higher fraction of Fe^{2+} species, compared to counterparts produced by conventional melting, consistent with our previous [57]Fe Mossbauer spectroscopy study. Laboratory and synchrotron Fe K-edge XANES data from the same suite of glass materials were found to be in excellent agreement. Accurate determination of Fe^{2+} / Σ Fe ratio by laboratory XANES analysis, will require careful calibration against centroid energy of the pre-edge features, due to the known non-linear dependence when both average oxidation state and co-ordination number vary at the same time. Nevertheless, this preliminary study has established that

laboratory XANES data are of sufficient resolution and sensitivity, in principle, to routinely probe Fe^{2+} / Σ Fe ratio in iron phosphate glasses and other materials.

5. References

[1]   NDA 2016 *Nuclear Decommissioning Authority Strategy effective from April 2016*
[2]   NDA/RWM 2016 *Geological Disposal Science and Technology Plan.*
[3]   NDA 2019 *5-year R&D Plan 2019 to 2024*
[4]   Hyatt N C and James M 2013 *Nucl. Eng. Int.* **2** 10-3
[5]   Bingham P A, Hyatt N C and Hand R J 2012 *Glass Technol. Part A* **53** 83.
[6]   Bingham P A, Hyatt N C, Hand R J and Forder S D 2013 *Glass Technol. Part A* **54** 1.
[7]   Bingham P A, Hyatt N C, Hand R J and Wilding C R 2009 *Mat. Res. Soc. Symp. P.* **1124** 161.
[8]   Heath P G, Corkhill C L, Stennett M C, Hand R J, Whales K M and Hyatt N C 2018 *J. Nucl. Mater.* **508** 203.
[9]   Hyatt N C, Morgan S, Stennett M C, Scales C R, Deegan D, 2007 *Mat. Res. Soc. Symp. P.* **985** 293
[10]   Hyatt N C, Schwarz R R, Bingham P A, Stennett M C, Corkhill C L, Heath P G, Hand R J, James M, Pearson A and Morgan S 2013 *J. Nucl. Mater.* **444** 186.
[11]   Brow R K, Kim C W and Reis S T 2020 *Int. J. Appl. Glass Sci.* **11** 4.
[12]   Day D E, Wu Z, Ray C S and Hrma P 1998 *J Non-Cryst. Solids* **241** 1.
[13]   Joseph K, Stennett M C, Hyatt N C, Asuvathraman R, Dube C L, Gandy A S, Kutty K V G, Jolley K, Rao P R V and Smith R 2017 *J. Nucl Mater.* **494** 342.
[14]   Kim C W and Day D E 2003 *J. Non-Cryst. Solids* **331** 20.
[15]   Mesko M G, Day D E and Bunker B C 2000 *Waste Manag.* **20** 271-8.
[16]   Marasinghe G K, Karabulut M, Ray C S, Day D E, Shumsky M G, Yelon W B, Booth C H, Allen P G and Shuh D K 1997 *J. Non-Cryst. Solids* **222** 144.
[17]   Karabulut M, Marasinghe G K, Ray C S, Day D E, Waddil G D, Booth C H, Allen P G, Bucher   J J, Caulder D L and Shuh D K 2002 *J. Non-Cryst. Solids* **306** 182.
[18]   Ray C S, Fang X, Karabulut M, Marasinghe G K and Day D E 1999 *J. Non-Cryst. Solids* **249** 1.
[19]   Fang X, Ray C S, Moguš-Milanković A and Day D E 2001 *J. Non-Cryst. Solids* **283** 162.
[20]   Griscom D L, Merzbacher C I, Bibler N E, Imagwa H, Uchiyama S, Namiki A, Marasinghe G K, Mesko M and Karabulut M 1998 *Nucl. Instr. and Meth. In Phys. Res. B* **141** 600.
[21]   Joseph K, Jolley K and Smith R 2015 *J. Non-Cryst. Solids*, **411** 137.
[22]   Jolley K and Smith R 2016 *Nucl. Instr. Methods Phys. Res. Sec. B.* **374** 8.
[23]   Forder S D, Bingham P A, McGann O J, Stennett M C and Hyatt N C 2013 *Hyperfine Interact.* **217** 83.
[24]   Waychunas G A, Apted M J and Brown G E 1983 *Phys. Chem. Miner.* **10** 1.
[25]   Bajit S, Sutton S R and Delaney J S 1994 *Geochim. Cosmochim. Acta* **58** 5209.
[26]   Galoisy L, Calas G and Arrio M A 2001 *Chem. Geol.* **174** 307.
[27]   Petit P E, Farges F, Wilke M and Solé V A 2001 *J. Synchrotron Radiat.* **8** 952.
[28]   Wilke M, Farges F, Petit P E, Brown G E and Martin F 2001 *Am. Mineral.* **86** 714.
[29]   Berry A J, O'Neill H S, Jayasuriya K D, Campbell S J and Foran G J 2003 *Am. Mineral.* **88** 967.
[30]   Mottram L M, Cafferkey S, Mason A R, Oulton T, Sun S K, Bailey D J, Stennett M C and Hyatt N C 2020 *J. Geosci.,* **65** 27.
[31]   Stennett M C and Hyatt N C 2009 *Mat. Res. Soc. Symp. P.* **1124** 147.
[32]   Mayzan M Z H, Stennett M C, Hyatt N C and Hand R J 2014 *J. Nucl. Mater.* **454** 343.
[33]   Arnold H 1986 *Z. Kristallogr. Cryst. Mater.* **177** 139.
[34]   Baum E, Treutmann W, Behruzi M, Lottermoser W and Amthauer G 1988 *Z. Kristallogr.* **183** 273.
[35]   Smyth J R 1975 *Am. Mineral.* **60** 1092.
[36]   Hawthorne F C, Ungaretti L, Oberti R, Caucia F and Callegari A 1993 *Can. Mineral.* **31** 551.
[37]   Seidler G T, Mortensen D R, Remesnik A J, Pacold J I, Ball N A, Barry N, Styczinski M and Hoidn O R 2014 *Rev. Sci. Instrum.* **85** 113906.
[38]   Seidler G T, Ditter A S, Ball N A and Remesnik A J 2016 *J. Phys. Conf. Ser.* **712** 012015.

[39] Mortensen D R, Seidler G T, Ditter A S and Glatzel P 2016 *J. Phys. Conf. Ser.* **712** 012036.

[40] Jahrman E P, Holden W M, Ditter A S, Mortensen D R, Seidler G T, Fister T T, Kozimor S A, Piper L F J, Rana J, Hyatt N C and Stennett M 2019 *Rev. Sci. Instrum.* **90** 024106.

[41] Mortensen D R and Seidler G T 2017 *J. Electron. Spectrosc. Relat. Phenom.* **215** 8.

[42] Ravel B and Newville M 2005 *J. Synchrotron Radiat.* **12** 537.

[43] Bearden J A and Burr A F 1967 *Rev. Mod. Phys.* **39** 125.

[44] Mottram L M, Dixon Wilkins M C, Blackburn L R, Oulton T, Stennett M C, Sun S K, Corkhill C L and Hyatt N C 2020 *MRS Adv.* **5** 27.

[45] Wang G, Wang Y and Jin B 1994 *Proc. SPIE* **2287** 214.

[46] Karabulut M, Marasinghe G K, Ray C S, Day D E, Waddill G D, Allen P G, Booth C H, Bucher J J, Caulder D L, Shuh D K, Grimsditch M, Saboungi M L 2000 *J. Mater. Res.* **15** 1972.

Acknowledgment